

# Prospects of phase-adaptive cooling of levitated magnetic particles in a hollow-core photonic-crystal fibre

P. Kumar,<sup>1,\*</sup> F. G. Jimenez,<sup>2</sup> S. Chakraborty,<sup>3,1</sup> G. K. L. Wong,<sup>1</sup> N. Y. Joly,<sup>3,1</sup> and C. Genes<sup>1,3</sup>

<sup>1</sup>Max Planck Institute for the Science of Light, Staudtstraße 2, D-91058 Erlangen, Germany

<sup>2</sup>Pontificia Universidad Católica del Perú, Av. Universitaria 1801, San Miguel 15088, Peru

<sup>3</sup>Department of Physics, Friedrich-Alexander-Universität Erlangen-Nürnberg, Staudtstraße 7, D-91058 Erlangen, Germany  
(Dated: October 4, 2024)

We analyze the feasibility of cooling of classical motion of a micro- to nano-sized magnetic particle, levitated inside a hollow-core photonic crystal fiber. The cooling action is implemented by means of controlling the phase of one of the counter-propagating fiber guided waves. Direct imaging of the particle's position, followed by the subsequent updating of the control laser's phase leads to Stokes type of cooling force. We provide estimates of cooling efficiency and final achievable temperature, taking into account thermal and detection noise sources. Our results bring forward an important step towards using trapped micro-magnets in sensing, testing the fundamental physics and preparing the quantum states of magnetization.

PACS numbers: 42.50.Ar, 42.50.Lc, 42.72.-g

## I. INTRODUCTION

Mechanical resonators are good actuators for displacement [1], force [2], acceleration [3] or mass sensing [4] applications. A prerequisite for sensing is the control of their motion to a level where fluctuations, either classical, such as stemming from thermal environments or quantum, are almost completely frozen. In the optomechanical realm [5], cooling of isolated mechanical resonances has been achieved both via cavity self-cooling [6–9], feedback in the form of cold-damping [10–15] or parametric modulation [16–21].

Magnetic micro-particles composed of yttrium iron garnet and yttrium orthoferite have been recently trapped inside photonic crystal fibers [22]. It is to be pointed out that unlike the optical levitation in free space [23], hollow-core photonic crystal fibre (HC-PCF) provides a novel platform for diffraction free trapping and guidance of micro- and nanoparticles over distances several orders of magnitude larger than the Rayleigh length of the trapping light [24–27]. Additionally, the environment surrounding the particle inside the hollow-core can also be tuned with inclusion of gas, vacuum or liquid [28, 29]. Owing to the large magnetization [30, 31] of the trapped particle, such a system holds the promise of providing excellent sensors for stray magnetic fields [32]. However, at moderate temperatures, their occupancy is at the level of  $10^{10}$  phonons, as their trapping frequency  $\Omega$  lies typically in the kilohertz regime. In addition, the gas pressure which is required to keep the particle stably trapped, around mbar, gives rise to a damping rate at the level of 300 Hz meaning that the mechanical quality factor is very low. However, further reduction of the pressure, desirable in order to increase the mechanical quality factor, causes the particle to escape from the trap

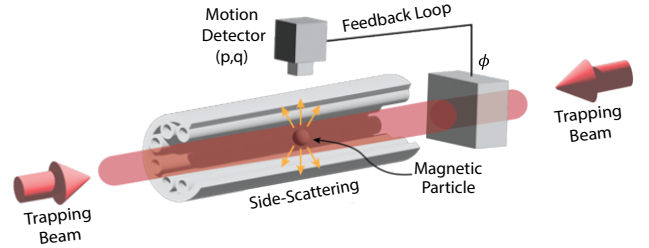


FIG. 1. A magnetic micro-sphere is trapped in the potential minimum of a standing wave inside a hollow-core optical photonic crystal fibre. The standing wave minima can be shifted in the  $y$ -direction of the fibre by the modification of the phase  $\phi(t)$  of the right-propagating guided control laser. Detection of the particle's position  $y_{\text{det}}(t)$  gives an estimate  $y(t)$  of the true value  $y(t)$ , with an additional noise term  $\eta W(t)$  modeled as a Wiener process  $W(t)$  multiplied by the efficiency of the imaging scheme (poorer resolution translates into a larger  $\eta$ ). Phase adaptive feedback results from the monitoring of the detected quadrature  $y_{\text{det}}$  and the subsequent adjustment of  $\phi$ .

due to increase in its bulk temperature and insufficient damping at low pressure [33].

We propose here an alternative route, where external optical damping is switched on during the pressure reduction stage and switched off in the next stage. This ensures the stability of the system and allows for the reach of very low pressures, where the particle is isolated from the thermal environment. The feedback loop involves a phase-adaptive mechanism [21], providing an effective Stokes-type damping force [34]. The feedback force comes from the continuous adjustment of the relative phase  $\phi(t)$  between the two counter-propagating trapping lasers (see Fig. 1). This consequently allows for a controllable shifting of the potential minimum and thus the particle's equilibrium position. In a first step, one detects light scattered to the side of the fibre and

\* pardeep.kumar@mpl.mpg.de

feeds the information into a motion controller. The deduced quantity is the particle's dimensionless position  $q_{\text{det}}(t) = q(t) + \eta W^{\text{det}}(t)$ , which contains the exact value of the position quadrature  $q(t)$ , to which one adds inherent detection noise of amplitude  $\eta$  and modelled as a Wiener process  $W^{\text{det}}(t)$  [35]. The detected signal is then used to estimate  $\phi(t) = (\mathcal{C}/\Omega)[q_{\text{det}}(t) - q_{\text{det}}(t - \tau)]/\tau$ , where  $\mathcal{C}$  and  $\tau$  are adjustable parameters. Subsequently, the phase deduced is used to control the right propagating laser, leading to the desired optical damping effect.

The paper is organized as follows. In Sec. II, we introduce the model and equations of motion for a classically trapped particle subject to stochastic noise stemming from the thermal environment and the dynamical adjustment of the phase. We then provide analytical solutions for the optical damping rate as well as for the final achievable occupancy in Sec. III. We model the backaction noise stemming from the action of the feedback loop. In Sec. IV, we provide experimental description for the system under consideration, an in-depth discussion on the tunability of the involved parameters to freeze thermal fluctuations from the system and validation of the results by accompanying numerical simulations. Finally, the concluding remarks are presented in Sec. V

## II. MODEL AND EQUATIONS

Let us assume that a magnetic particle of mass  $m$  is trapped in the standing wave formed by two counter-propagating waves with frequency  $\omega_\ell$  and wave-vector  $\pm k_\ell$  along the  $y$ -direction. The plus component of the electric field amplitude can be expressed as a superposition of  $\mathcal{E}_0 e^{ik_\ell y} e^{-i\omega_\ell t}$  and  $\mathcal{E}_0 e^{-ik_\ell y} e^{-i\omega_\ell t} e^{-2i\phi(t)}$  counterpropagating waves, where  $\mathcal{E}_0$  and  $\phi(t)$  are the amplitude and the relative phase of the light fields. In a frame rotating at  $\omega_\ell$ , the total electric field is then  $\mathcal{E}(y, t) = 2\mathcal{E}_0 \cos[k_\ell y + \phi(t)]$ . This leads to a position and time dependent potential energy  $-\alpha' \mathcal{E}(y, t)^2/4$  for the particle, where  $\alpha'$  represents the real part of the particle's polarisability. This allows in turn for the computation of the gradient optical force, in the  $y$ -direction, to be obtained as

$$F_y = \alpha' |\mathcal{E}_0|^2 \frac{\partial}{\partial y} \left[ \cos(k_\ell y + \phi(t)) \right]^2. \quad (1)$$

Assuming that the particle is trapped in the minimum of the optical potential, it is easy to decompose the force into the following two contributions

$$F_y = - \left[ 2k_\ell^2 \alpha' |\mathcal{E}_0|^2 \right] y - \left[ 2k_\ell \alpha' |\mathcal{E}_0|^2 \right] \phi(t). \quad (2)$$

The first term in above equation is the restoring force, indicating a spring (or trapping) constant  $k_{\text{trap}} = 2k_\ell^2 \alpha' |\mathcal{E}_0|^2 = m\Omega^2$ . This way we set the value of the optical trap frequency  $\Omega$  and note that it can be adjusted solely by tuning the laser power, as the mass  $m$  and the

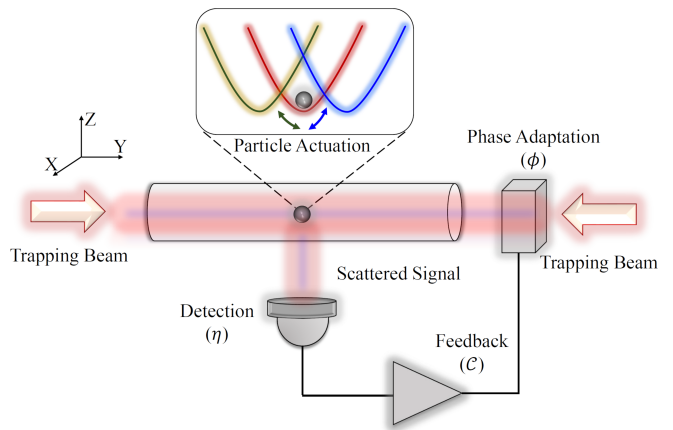


FIG. 2. Detailed scheme showing the important parameters involved in the feedback loop, such as the imaging factor  $\eta$  and the feedback amplification factor  $\mathcal{C}$ . The inset shows the shifting of the trap minimum (red harmonic potential) from the equilibrium position to the left (green) and right (blue) via the control of the right pump phase  $\phi$ . This control knob allows for the emergence of a Stokes-like optical damping force, acting to cool the particle's motion.

real part of the polarizability  $\alpha'$  are fixed values for a given material used. The second term is an additional time-dependent force, arising due to the relative phase difference between the counter-propagating fields and expressed in a simpler form as  $F_{\text{add}} = -(k_{\text{trap}}/k_\ell)\phi(t)$ . By adjusting the right pump's phase  $\phi$ , this force acts as an actuator by shifting the trap minimum from its equilibrium position, in such a way to counteract its motion when desired, as shown in the inset of Fig. 2.

We can now proceed in writing the difference equations for the oscillator subject to the additional force stemming from the dynamical adjustment of the phase  $\phi(t)$  and to thermal noise as

$$dq = \Omega p dt, \quad (3a)$$

$$dp = -\gamma p dt - \Omega q dt - \beta \phi(t) dt + \sqrt{2\gamma n_{\text{th}}} dW^{\text{th}}(t). \quad (3b)$$

In doing so we have reduced the description to dimensionless quadratures  $y = y_{\text{zpm}} q$  and  $p = p_{\text{zpm}} p$  where the zero-point motion for the position is  $y_{\text{zpm}} = \sqrt{\hbar/(m\Omega)}$  (the extent of the wavefunction at zero temperature) and for the momentum  $p_{\text{zpm}} = \sqrt{\hbar m \Omega}$ . Also, we introduced the notation  $\beta = k_{\text{trap}}/(k_\ell p_{\text{zpm}})$ , with dimensions of frequency. The Wiener increment for the thermal environment has zero average and only surviving correlations  $\langle dW^{\text{th}}(t) dW^{\text{th}}(t) \rangle = dt$  at equal times (all correlations at different times vanish). The thermal occupancy corresponding to a bath of temperature  $T_{\text{th}}$  (assumed large) is written as  $n_{\text{th}} \approx k_B T_{\text{th}}/(\hbar\Omega)$ . For example, assuming  $\Omega/2\pi = 1$  kHz and  $T_{\text{th}} = 300$  K, one obtains  $n_{\text{th}} = 10^{10}$ , very far from the quantum regime. From Eqs. (3), it can be easily verified that in the absence of additional actuation force, the system achieves equilibrium at a rate  $\gamma$  with its thermal environment at temperature  $T_{\text{th}}$  (see

Appendix C for details).

We provide now a quasi-derivative feedback cooling procedure, where the phase of the control laser is assumed to be

$$\phi(t) = \frac{C}{\Omega} \times \frac{q_{\text{det}}(t) - q_{\text{det}}(t - \tau)}{\tau}. \quad (4)$$

Here  $C$  is the feedback amplification factor: larger values lead to faster cooling but also increased detection noise. The time interval  $\tau$  is the interval on which the quasi-derivative operation is performed. A direct cold-damping feedback is obtained by setting  $\tau = dt$  and letting  $dt \rightarrow 0$ . The detection noise is modelled by the inclusion of a Wiener process to the true value of the position and multiplied by an amplitude  $\eta$  such that at any time  $q_{\text{det}}(t) = q(t) + \eta W^{\text{det}}(t)$ . This allows to estimate the best strategy in terms of the choice of  $\tau$  and in terms of the optimal magnitudes of  $C$  and  $\eta$ . We will address this procedure in Sec. III and estimate both the cooling rate as well as final occupancy encompassing both thermal and measurement noise contributions.

### III. THEORY OF QUASI-DERIVATIVE COOLING

We will separate our analysis in two parts by first deducing an analytical expression for the optical feedback cooling rate and afterwards estimating the added measurement noise and the corresponding final achievable occupancy. In a first step we solely consider deterministic motion (no thermal or measurement noise) and deduce the feedback effect in adding an extra cooling rate  $\bar{\Gamma}$  to  $\gamma$ . In the second step, we estimate the contributions of both (uncorrelated) noise sources, detection and thermal, and deduce the effective occupancy incorporating both effects.

#### A. Cooling rate

To obtain the modified cooling rate, we take into account of the deterministic part of Eqs. (3) and neglect the influence of noise. This allows us to write the following set of coupled differential equations

$$\frac{dq}{dt} = \Omega p, \quad (5a)$$

$$\frac{dp}{dt} = -\gamma p - \Omega q - \beta \phi(t). \quad (5b)$$

A formal integration of the first equation for the displacement quadrature yields  $q(t) = q(t - \tau) + \Omega \int_{t-\tau}^t p(t') dt'$ . Assuming that the effect of the feedback is not too strong in the interval from  $t - \tau$  to  $t$  (which is valid when restricting values of  $\tau$  of the order of the mechanical period

$T = 2\pi/\Omega$ , or smaller), one can assume, in first order, that only natural evolution at frequency  $\Omega$  and damping rate  $\gamma$  occurs in this interval  $t - \tau$  to  $t$ . This allows one to deterministically connect  $p(t')$  with  $p(t)$  and  $q(t)$ . After performing the integration of decaying, oscillating terms (see Appendix A), one sees a modification of the effective decay rate from the purely thermally induced  $\gamma$  to the optically modified one  $\gamma + \bar{\Gamma}$  (by identifying the terms proportional to  $p(t)$ ) where

$$\bar{\Gamma} = \beta C \left[ e^{\gamma\tau/2} \frac{\sinh \Omega\tau}{\Omega\tau} \right]. \quad (6)$$

For  $\tau \rightarrow 0$ , we recover an expected cold-damping type of result with a derivative feedback showing an optimal value  $\Gamma = \beta C$ .

In addition to damping, the mechanical resonance frequency is also modified via an optical spring effect, which we obtain from the identification of the extra factors in front of  $q(t)$  leading to

$$\bar{\Omega} = \Omega - \beta C \left[ \frac{e^{\gamma\tau/2} \cosh \Omega\tau - 1}{\Omega\tau} \right] + \frac{\gamma\bar{\Gamma}}{2\Omega}. \quad (7)$$

In the limit of small  $\tau$ , the optical spring effect cancels out  $\bar{\Omega} = \Omega$ . However, for finite  $\Omega\tau$ , this indicates an additional tuning knob for reducing the effective occupancy, by increasing the oscillator frequency.

#### B. Final occupancy

Let us now analyze how measurement noise enters the equation of motion Eq. (3b) via the term  $-\beta\phi(t)dt$ . This can be written in the difference equations form as

$$\mathcal{N}^{\text{det}}(t) = -\frac{\eta\beta C}{\Omega} \left[ \frac{W^{\text{det}}(t) - W^{\text{det}}(t - \tau)}{\tau} \right] dt. \quad (8)$$

and to be added to the standard thermal noise  $\sqrt{2\gamma n_{\text{th}}} dW^{\text{th}}(t)$ . By expressing the Wiener process entering the detection as a discrete sum over Wiener increments [see Fig. 3] with infinitesimal increment of time  $dt$  (such that  $t = ndt$  and  $\tau = n_{\tau}dt$ ), we can rewrite

$$\mathcal{N}^{\text{det}}(t) = -\frac{\eta\beta C dt}{\Omega\tau} \sum_{m=1}^{n_{\tau}} dW_{n-n_{\tau}+m}^{\text{det}}. \quad (9)$$

In order to estimate the contribution of the two types of noises to the steady state of the system, we follow the derivation shown in Ref. [21] and detailed in Appendix B. The steady state solution for the momentum is obtained by taking the large  $n$  limit and reads

$$p_n = \frac{1}{\bar{\gamma}_+ - \bar{\gamma}_-} \sum_{j=0}^{n-1} \left( \mathcal{N}_j^{\text{det}} + \sqrt{2\gamma n_{\text{th}}} dW_j^{\text{th}} \right) \left( \bar{\gamma}_+ \bar{\lambda}_+^j - \bar{\gamma}_- \bar{\lambda}_-^j \right), \quad (10)$$

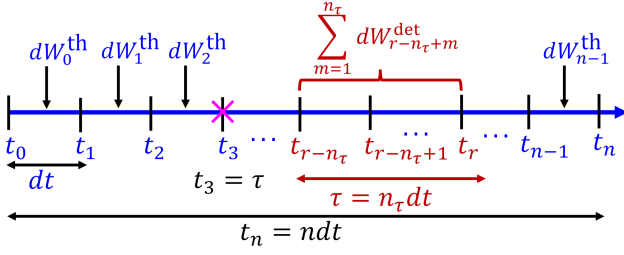


FIG. 3. Schematic depicting the time steps in which thermal and measurement back-action noise are included during the time evolution. The time interval  $[t_0, t_n]$  is chopped into  $n$  infinitesimal intervals of length  $dt = t_n/n$ . The thermal noise increments,  $dW_j^{\text{th}}$  ( $j = 0, 1 \dots n-1$ ), are added in each time-step. The phase adaptive feedback starts at time  $\tau$  shown by magenta cross and is discretized into  $n_\tau$  steps of duration  $dt$ . The measurement noise is added as sum over Wiener increments for each evolution step, once the feedback starts acting. One of such an interval from  $t_{r-n_\tau}$  to  $t_r$  is shown in red during which the Wiener increments  $\sum_{m=1}^{n_\tau} dW_{r-n_\tau+m}^{\text{det}}$  are included.

where the coefficients are obtained from the eigenvalues,  $\bar{\lambda}_\pm = 1 - \bar{\gamma}_\pm dt/2$ , of the evolution matrix. Here

$$\bar{\gamma}_\pm = \bar{\gamma} \pm \sqrt{\bar{\gamma}^2 - 4\bar{\Omega}^2}, \quad (11)$$

contain the renormalized damping rate  $\bar{\gamma} = \gamma + \bar{\Gamma}$  and frequency  $\bar{\Omega}$ . The aim is to compute the variance  $\langle p_n^2 \rangle$  in steady state. As the two noises are uncorrelated one can separate two contributions  $\langle p_n^2 \rangle = \langle p_n^2 \rangle_{\text{th}} + \langle p_n^2 \rangle_{\text{det}}$  and proceed by estimating each of them independently.

In a first step, we use the thermal noise correlations  $\langle dW_j^{\text{th}} dW_{j'}^{\text{th}} \rangle = dt \delta_{jj'}$  and make use of the following identities  $\lim_{n \rightarrow \infty} \sum_{j=0}^{n-1} \bar{\lambda}_\pm^{2j} = 1/(\bar{\gamma}_\pm dt)$ , and  $\lim_{n \rightarrow \infty} \sum_{j=0}^{n-1} \bar{\lambda}_+^j \bar{\lambda}_-^j = 2/[(\bar{\gamma}_+ + \bar{\gamma}_-) dt]$  (for details see Appendix B). This gives the correct estimate of the thermal final occupancy of the oscillator undergoing extra damping at rate  $\bar{\Gamma}$  and modified frequency  $\bar{\Omega}$ :

$$\langle p_n^2 \rangle_{\text{th}} = \frac{\gamma n_{\text{th}}}{\bar{\gamma}} \left( \frac{\bar{\Omega}}{\Omega} \right). \quad (12)$$

As expected, the initial large occupancy is reduced to the ratio of the thermalization rate  $\gamma n_{\text{th}}$  divided by the effective total damping rate  $\bar{\gamma}$  but with a modification resulting from optical spring effect [36]. In conventional feedback techniques, the final thermal occupancy can be reduced by increasing the damping rate. On top of this, enhanced resonant frequency provides an additional cooling [37]. The combined result of these two effects can yield very low thermal occupancy.

Let us now compute the steady state correlations of the detection noise  $\langle p_n^2 \rangle_{\text{det}}$ . First we introduce  $\mathcal{A} = -\eta\beta C dt / (\Omega\tau)$  and rewrite  $\mathcal{N}_j = \mathcal{A} \sum_{m=1}^{n_\tau} dW_{j-n_\tau+m}^{\text{det}}$ . Taking into account that the correlations  $\langle dW_{j-n_\tau+m}^{\text{det}} dW_{j'-n_\tau+m'}^{\text{det}} \rangle$  will impose the constraint  $j+m = j'+m'$  leads us to the following expression for the detection induced noise in the momentum

quadrature

$$\langle p_n^2 \rangle_{\text{det}} = \frac{\mathcal{A}^2 dt}{(\bar{\gamma}_+ - \bar{\gamma}_-)^2} \sum_{j=0}^{n-1} \sum_{m,m'=0}^{n_\tau} [f_j - g_j^{m-m'}], \quad (13)$$

where

$$f_j = \bar{\gamma}_+^2 \bar{\lambda}_+^{2j} + \bar{\gamma}_-^2 \bar{\lambda}_-^{2j}, \quad (14)$$

and

$$g_j^{m-m'} = \bar{\gamma}_- \bar{\gamma}_+ \bar{\lambda}_+^j \bar{\lambda}_-^j (\bar{\lambda}_-^{m-m'} + \bar{\lambda}_+^{m-m'}). \quad (15)$$

After evaluating the summation in above equations (see Appendix B for detailed derivations) we can approximate

$$\langle p_n^2 \rangle_{\text{det}} = \frac{1}{\bar{\gamma}} \left[ \frac{\sqrt{8\eta\beta C}}{\Omega\tau} \right]^2 \left[ \frac{\sinh^2\left(\frac{\bar{\gamma}_+\tau}{4}\right)}{\bar{\gamma}_+(\bar{\gamma}_+ - \bar{\gamma}_-)} - \frac{\sinh^2\left(\frac{\bar{\gamma}_-\tau}{4}\right)}{\bar{\gamma}_-(\bar{\gamma}_+ - \bar{\gamma}_-)} \right] \quad (16)$$

This tells us how the effective temperature is modified via the measurement back-action. One needs to then optimize  $\tau$  such that cooling rate is still high while the noise is minimized. Further, we will assume here equipartition between the variance of the position and the momentum and then derive the effective occupancy  $\bar{n} = \langle p_n^2 \rangle$ . Finally, one can list the fully analytical expression of the final occupancy as

$$\bar{n} = \frac{\gamma n_{\text{th}}}{\gamma + \bar{\Gamma}} \left( \frac{\bar{\Omega}}{\Omega} \right) + \frac{1}{\gamma + \bar{\Gamma}} \left[ \frac{\sqrt{8\eta\beta C}}{\Omega\tau} \right]^2 \left[ \frac{\mathcal{A}_+ - \mathcal{A}_-}{\bar{\gamma}_+ - \bar{\gamma}_-} \right], \quad (17)$$

where we introduce new notations as

$$\mathcal{A}_\pm = \frac{1}{\bar{\gamma}_\pm} \sinh^2\left(\frac{\bar{\gamma}_\pm\tau}{4}\right). \quad (18)$$

Notice that in the limit of  $\tau \rightarrow 0$ , the expression above simplifies to

$$\bar{n} \approx \frac{\gamma n_{\text{th}}}{\gamma + \beta C} + \frac{\left(\frac{\eta\beta C}{\sqrt{2}\Omega}\right)^2}{\gamma + \beta C}. \quad (19)$$

In this limit,  $\bar{\Omega} \approx \Omega$  and one recovers a standard result in optomechanics where the thermal occupancy is reduced to the ratio of the heating  $\gamma n_{\text{th}}$  to the externally imposed cooling rate added to the intrinsic damping rate  $\gamma + \beta C$ . The second term is the inadvertently added feedback noise, scaling with  $\eta^2$ . We will discuss the implications of this expression in the following section.

#### IV. DISCUSSIONS

Let us address here the feasibility of such a scheme to cool the classical thermal motion of a magnetic micro-sphere levitated inside the optical hollow-core fibre. To this end we connect to the experimental setup



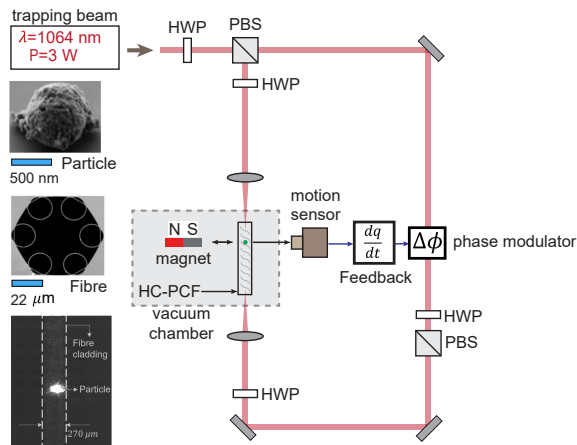


FIG. 4. Schematic of the experimental setup. HWP: half-wave plate, PBS: polarizing beam splitter. The fibre is placed inside a vacuum chamber capable of reaching ultra-high vacuum. A permanent magnet is mounted on a translational stage and can be moved back and forth radially relative to the fibre in order to adjust the amplitude of the magnetic field applied to the trapped particle. Insets: Scanning electron micrographs showing the cross-section of the HC-PCF with  $44 \mu\text{m}$  core diameter, the  $1 \mu\text{m}$  magnetic microparticle, and snapshot of an optically trapped magnetic particle inside the core of a HC-PCF captured with a high-speed camera. The motion sensor is a quadrant photodiode which detects the position quadrature of the levitated particle.

described in Ref. [22], making use of some of the parameters relevant for current experiments. We optimize the resulting expression for the final occupancy by taking into account the influence of gas pressure and we describe a procedure for feedback implementation. The validity of the analytical estimates is checked against numerical simulations of the stochastic difference equations.

### A. Experimental considerations

Let us refer to the setup in Ref. [22] where a magnetic microparticle is optically levitated inside a chiral single-ring HC-PCF at low pressure. A schematic of the setup is shown in Fig. 4 along with the insets showing the scanning electron micrographs of the magnetic microparticle, the HC-PCF and snapshot of an optically trapped magnetic particle captured with a high-speed camera. A linearly polarized laser beam at  $1064 \text{ nm}$  with  $3 \text{ W}$  of the total optical power is used to trap the magnetic particle inside the hollow core of the fibre. The mechanical quadratures of the particle can be detected by collecting the scattered light from the particle coming out of the fibre cladding as shown in the inset of Fig. 4 and focusing it onto a quadrature position sensor. Under ambient conditions of pressure, the particle's motion is heavily damped due to collisions with the background gas. However, the system

can be put in the underdamped oscillating regime once the fibre is evacuated using a vacuum chamber. In our experimental setup, at  $1 \text{ mbar}$ , underdamped motion of the particle is confirmed by detecting a Lorentzian spectrum of motion along  $y$ -axis, as shown in Fig. 5. The measured spectrum provides a resonance peak at a frequency  $\sim 2\pi \times 1 \text{ kHz}$  and damping rate of  $2\pi \times 0.3 \text{ kHz}$ . The noise floor in the spectrum has a value  $7.5 \text{ pm}/\sqrt{\text{Hz}}$  and the additional spikes in the spectrum arise due to the electronic noise from the detectors and data collection.

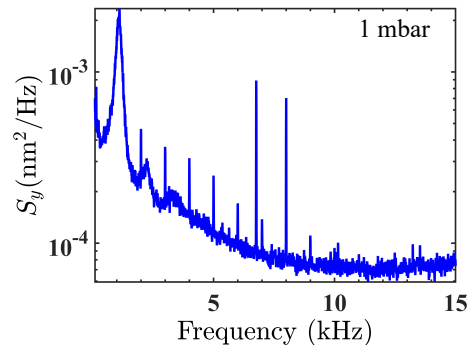


FIG. 5. Experimental spectrum of the damped mechanical motion of the bound magnetic particle at a pressure of  $1 \text{ mbar}$ . The resonance peak at  $\sim 1 \text{ kHz}$  corresponds to the underdamped motion of the particle. The additional spikes shown in the spectrum are electronic noise from our detectors and data collection. The laser power is  $3 \text{ W}$ .

### B. Optimizing the final occupancy

In above described setup, the magnetic microparticle can be stably trapped until around  $1 \text{ mbar}$ . However, after this it escapes from the trap due to an increase in internal bulk temperature of the particle and insufficient damping at low pressure [33]. This not only restricts the experiment to be performed at a pressure below  $1 \text{ mbar}$  but also limits its quality factor. A possible solution to these limitations can be provided by using the phase-adaptive feedback operation in order to keep the particle stable in the optical trap during the vacuum chamber evacuation procedure. As shown in Eq. (17), the final phonon occupancy in the system is limited by the product  $\eta\beta\mathcal{C}$ . Experimentally, the parameter  $\beta$  can be controlled by the trap stiffness which in turn can be adjusted by parameters such as the trapping power, and core size of the fibre. For the setup in Ref. [22],  $\beta = k_{\text{trap}}/(k_{\text{I}}p_{\text{zpm}}) = (\sqrt{m}\Omega^{3/2}\lambda_{\text{I}})/(2\pi\sqrt{\hbar}) = 6.4 \times 10^8 \text{ Hz}$ . The amplifier gain  $\mathcal{C}$  can be set to an optimum value in order to avoid subsequent additive noise while maintaining optimum signal-noise ratio during the stages of detection and feedback. To obtain this factor, we take  $\tau \rightarrow 0$  in Eq. (4). This leads to  $\phi = \mathcal{C}p_{\text{det}} \approx \mathcal{C}\sqrt{n_{\text{th}}}$ , where in a thermal state the variance of the momentum quadrature is taken to be  $n_{\text{th}}$ . The upper bound of the detected phase is  $2\pi$ . Using this, we

can estimate the maximum value of the gain parameter as  $C_{max} = 2\pi/\sqrt{n_{th}}$ . The noise floor for our current detection scheme is  $7.5 \text{ pm}/\sqrt{\text{Hz}}$  [see Fig. 5] and from this we can obtain the parameter  $\eta$ . To do so, we take into account of the spectral contribution due to detection noise (see appendix D for details) and around  $\omega \approx \Omega$ , we find  $\eta = 2 \times 10^4 \sqrt{\text{Hz}}$ .

Under low-vacuum conditions, the motion of trapped particle is strongly damped due to instantaneous collisions with the background gas and its energy quickly thermalizes with the environment at a rate  $\gamma$ . The momentum damping rate of the levitated particle can be reduced by decreasing the air pressure. From kinetic theory the damping constant follows the relation [26, 38]

$$\gamma = \frac{12\pi R}{m} \frac{\mu_0}{1 + \text{Kn}(\beta_1 + \beta_2 e^{-\beta_3/\text{Kn}})}, \quad (20)$$

where  $R$  is the particle radius, and  $m$  is its mass and  $\mu_0 = 18.1 \times 10^{-6} \text{ Pa}\cdot\text{s}$  is the coefficient of viscosity of air,  $\beta_1 = 1.231$ ,  $\beta_2 = 0.469$ , and  $\beta_3 = 1.178$  at the atmospheric pressure. Further in Eq. (20), the Knudsen number  $\text{Kn} = \frac{\lambda_{mfp}}{R} \propto \frac{1}{pR}$  is expressed as a ratio of the mean free path of the background gas to the radius of the particle, where  $p$  is the pressure of the surrounding gas. It can be verified from Eq. (20) that the damping of the trapped particle is independent of pressure in high-pressure regime where its motion gets over-damped due to strong interaction with the background gas. Contrary to this, for low-pressure, the mean free path becomes much larger than the radius of the particle and the damping in this regime varies linearly with pressure. Let us now refer to full numerical simulations corresponding to small  $\tau$ . We show in Fig. 6 sample trajectories obtained from integrating the set of Eqs. (3) in the presence of both thermal and feedback noise modelled using Wiener increments (see Appendix C for details of numerical procedure). The phonon occupancy is plotted for  $\tau/T = 1.6 \times 10^{-5}$  and for different pressures. In the absence of external damping and at a moderate pressure  $p = 2.6 \text{ mbar}$ , the phonon-occupancy is dominated by the stochastic Brownian thermal noise and the oscillator remains in equilibrium with its thermal environment. As shown in Fig. 6, when the phase-adaptive feedback cooling is switched on, the initial high phonon occupancy decays at the analytically predicted cooling rate  $\bar{\Gamma}$  and eventually saturates at a final value  $\bar{n}$  governed by and validating our analytical expression in Eq. (17). The equilibrium is reached due to the competition between the thermal reheating and the measurement backaction.

As the pressure is reduced further, the initial high thermal phonon occupancy decays rapidly within few oscillation periods of the oscillator as depicted in Fig. 6. For instance, at  $0.26 \mu\text{bar}$  of pressure, the phonon population can be reduced to the level of  $10^5$  from the initial high occupation of  $10^{10}$ . This can further be understood in terms of phase-space representation plotted in Figs. 6(b) and (c) for a pressure of  $0.26 \mu\text{bar}$ . Due to the applied feedback,

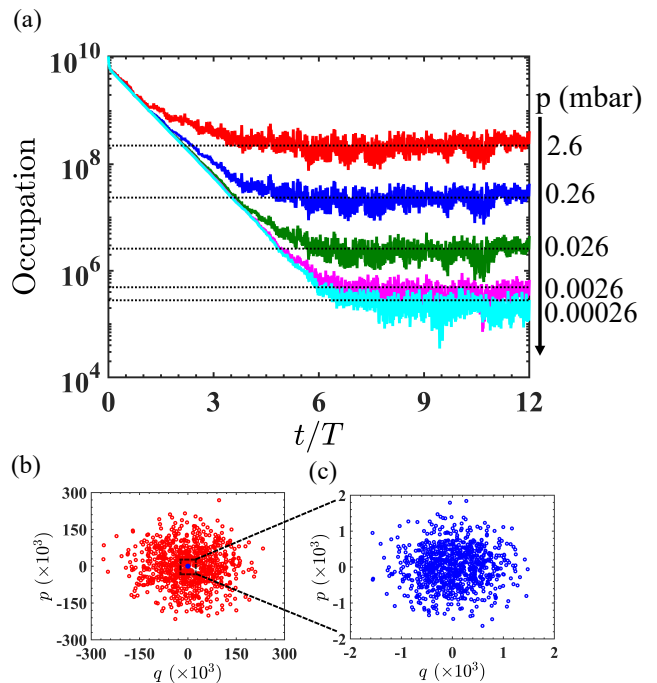


FIG. 6. Phase adaptive feedback cooling. (a) Temporal evolution of the phonon occupancy for different pressures. The occupancy is obtained from a numerical simulation of Eqs. (3) taking into account both thermal and detection noises along with the pressure dependence governed by Eq. (20). The dotted lines show the validity of the analytically predicted final occupancy given by Eq. (17). (b) Phase-space representation of an initial thermal state (red points) and the cooling state (blue points) obtained for  $p = 0.26 \mu\text{bar}$ , and (c) for a corresponding pressure, enlarged view of the thermal distribution of the final cold state. Parameters used are  $\Omega/2\pi = 1 \text{ kHz}$ ,  $T = 2\pi/\Omega$ ,  $\tau/T = 1.6 \times 10^{-5}$ ,  $T_{th} = 300 \text{ K}$ ,  $n_{th} = 6.3 \times 10^9$ ,  $\beta/2\pi = 102 \text{ MHz}$ ,  $C = C_{max} = 2\pi/\sqrt{n_{th}}$ ,  $\eta = 2 \times 10^4 \sqrt{\text{Hz}}$ ,  $\mu_0 = 18.1 \text{ Pa}\cdot\text{s}$ , density of YIG =  $5.11 \text{ g/cm}^3$ , and  $R = 0.66 \mu\text{m}$ .

the thermal distribution of variance  $n_{th}$  corresponding to an initial hot state suppresses in phase-space to an analogous distribution of reduced variance  $\bar{n}$  associated with a final cold state. Notice that the phase space result validate the assumption that equipartition applies even in the presence of externally controlled damping. For larger values of  $\tau$ , the scheme describes a quasi-derivative feedback regime instead of an instantaneous cold-damping operation. At  $0.26 \mu\text{bar}$ , in Fig. 7, we compare the phonon occupation obtained from two feedback operations for  $\tau/T = 1.6 \times 10^{-5}$  and  $\tau/T = 4.8 \times 10^{-2}$ . Interestingly, the quasi-derivative scheme performs well albeit the final phonon occupation remains slightly higher than the cold damping. It is due to the increase in detection noise over longer time-intervals of feedback operation. Further, while tuning  $\tau$ , we ensured the stability of the system. However, we observe that around  $\tau/T \approx 0.1$ , when  $\bar{\gamma} \approx 2\bar{\Omega}$ , the system becomes dynamically unstable. This restricts the values of  $\tau$  ( $< 0.1T$ ) for the efficient feedback operation. These remarks suggest that in our phase-adaptive

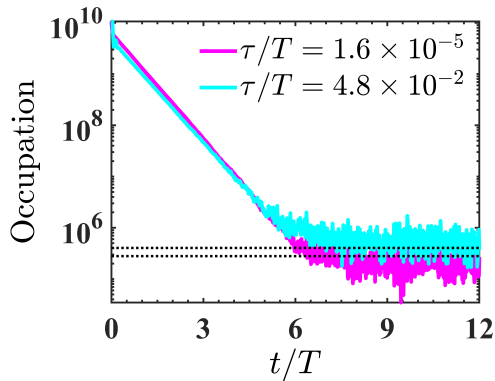


FIG. 7. Plot of the phonon occupancy as a function of time at  $0.26 \mu\text{ bar}$  for  $\tau/T = 1.6 \times 10^{-5}$  (solid magenta line) and  $\tau/T = 4.8 \times 10^{-2}$  (solid cyan line). The results are extracted from numerical simulations of Eqs. (3). The dotted lines illustrate the analytically predicted final occupancy values. Other parameters used are same as in Fig. 6.

mechanism, the effective Stokes-type damping force (when  $\tau \rightarrow 0$ ) offers a best strategy for the isolation from thermal bath.

### C. Feedback implementation

Let us remark at the possible experimental strategy to implement such a phase adaptive feedback cooling mechanism, for the setup described in Fig. 4. The magnetic particle is trapped inside a hollow core fibre by using a linearly polarized laser beam of power 3 W and wavelength 1064 nm at an initial pressure of 10 mbar. Due to collinear polarisation states of the tweezer arms, a standing wave pattern is formed inside the fibre. The starting point of the phase-adaptive feedback cooling is to detect the time varying position quadrature of the particle. This can be accomplished by imaging the particle by collecting the scattered light coming out of the fibre cladding [see inset of Fig. 4]. The collected light is then focused onto a

quadrant position sensor from which a signal would be filtered out by a bandpass filter centered around  $2\pi \times 1$  kHz, followed by a derivative circuit, a variable gain amplifier and a phase shifter. The output signal goes to the phase-modulator such as a Pockels cell. The Pockels cell will modulate the phase of the trapping beam in one of the tweezer arms in order to shift the standing wave pattern proportional to the instantaneous velocity of the levitated particle inside the HC-PCF.

## V. CONCLUSIONS

We presented the prospects of cooling the thermal excess fluctuations linked to the mechanical motion of a magnetic microparticle, optically levitated inside a hollow-core photonic crystal fibre and in the presence of a thermal gas. The cooling is achieved through an engineered phase-adaptive feedback loop that provides an effective Stokes type viscous damping force to the system. This is accomplished by directly imaging the particle's position followed by the adjustment of relative phase between two counter-propagating fibre guided waves. We provided an analytical estimate of the final phonon occupation taking into account of thermal as well as the measurement noises. Our numerical simulations validate the analytical results. Our findings are consequential for using trapped magnetic particles as sensors for feeble stray magnetic fields [32]. Future work analysing the feasibility of reaching the quantum ground state will aim at extending this procedure to prepare the non-classical states of magnetization [39–41] and testing aspect of fundamental quantum physics [42, 43].

## ACKNOWLEDGMENTS

We acknowledge financial support from the Max Planck Society and the Deutsche Forschungsgemeinschaft (DFG, German Research Foundation) – Project-ID 429529648 – TRR 306 QuCoLiMa (“Quantum Cooperativity of Light and Matter”).

- 
- [1] G. Anetsberger, O. Arcizet, Q. P. Unterreithmeier, R. Rivière, A. Schliesser, E. M. Weig, J. P. Kotthaus, and T. J. Kippenberg, “Near-field cavity optomechanics with nanomechanical oscillators,” *Nature Physics* **5**, 909 (2009).
  - [2] F. Fogliano, B. Besga, A. Reigue, L. Mercier de Lépinay, P. Heringlake, C. Gouriou, E. Eyraud, W. Wernsdorfer, B. Pigeau, and O. Arcizet, “Ultrasensitive nano-optomechanical force sensor operated at dilution temperatures,” *Nature Communications* **12**, 4124 (2021).
  - [3] A. G. Krause, M. Winger, T. D. Blasius, Q. Lin, and O. Painter, “A high-resolution microchip optomechanical accelerometer,” *Nature Photonics* **6**, 768 (2012).
  - [4] M. Sansa, M. Defoort, A. Brenac, M. Hermouet, L. Banniard, A. Fafin, M. Gely, C. Masselon, I. Favero, G. Jourdan, and S. Hentz, “Optomechanical mass spectrometry,” *Nature Communications* **11**, 3781 (2020).
  - [5] M. Aspelmeyer, T. J. Kippenberg, and F. Marquardt, “Cavity optomechanics,” *Rev. Mod. Phys.* **86**, 1391 (2014).
  - [6] U. Delić, M. Reisenbauer, D. Grass, N. Kiesel, V. Vuletić, and M. Aspelmeyer, “Cavity cooling of a levitated nanosphere by coherent scattering,” *Phys. Rev. Lett.* **122**, 123602 (2019).
  - [7] U. Delić, M. Reisenbauer, K. Dare, D. Grass, V. Vuletić, N. Kiesel, and M. Aspelmeyer, “Cooling of a levitated nanoparticle to the motional quantum ground state,” *Sci-*

- ence **367**, 892 (2020).
- [8] D. Windey, C. Gonzalez-Ballester, P. Maurer, L. Novotny, O. Romero-Isart, and R. Reimann, “Cavity-based 3D cooling of a levitated nanoparticle via coherent scattering,” *Phys. Rev. Lett.* **122**, 123601 (2019).
- [9] C. Gonzalez-Ballester, P. Maurer, D. Windey, L. Novotny, R. Reimann, and O. Romero-Isart, “Theory for cavity cooling of levitated nanoparticles via coherent scattering: Master equation approach,” *Phys. Rev. A* **100**, 013805 (2019).
- [10] T. Li, S. Kheifets, and M. G. Raizen, “Millikelvin cooling of an optically trapped microsphere in vacuum,” *Nature Physics* **7**, 527 (2011).
- [11] J. Millen, T. S. Monteiro, R. Pettit, and A. N. Vamivakas, “Optomechanics with levitated particles,” *Reports on Progress in Physics* **83**, 026401 (2020).
- [12] M. Rossi, D. Mason, J. Chen, Y. Tsaturyan, and A. Schliesser, “Measurement-based quantum control of mechanical motion,” *Nature* **563**, 53 (2018).
- [13] F. Tebbenjohanns, M. L. Mattana, M. Rossi, M. Frimmer, and L. Novotny, “Quantum control of a nanoparticle optically levitated in cryogenic free space,” *Nature* **595**, 378 (2021).
- [14] L. Magrini, P. Rosenzweig, C. Bach, A. Deutschmann-Olek, S. G. Hofer, S. Hong, N. Kiesel, A. Kugi, and M. Aspelmeyer, “Real-time optimal quantum control of mechanical motion at room temperature,” *Nature* **595**, 373 (2021).
- [15] C. Whittle and et al, “Approaching the motional ground state of a 10-kg object,” *Science* **372**, 1333 (2021).
- [16] L. G. Villanueva, R. B. Karabalin, M. H. Matheny, E. Kenig, M. C. Cross, and M. L. Roukes, “A nanoscale parametric feedback oscillator,” *Nano Lett.* **11**, 5054 (2012).
- [17] J. Gieseler, B. Deutsch, R. Quidant, and L. Novotny, “Subkelvin parametric feedback cooling of a laser-trapped nanoparticle,” *Phys. Rev. Lett.* **109**, 103603 (2012).
- [18] J. Gieseler, L. Novotny, and R. Quidant, “Thermal nonlinearities in a nanomechanical oscillator,” *Nature Physics* **9**, 806 (2013).
- [19] B. Rodenburg, L. P. Neukirch, A. N. Vamivakas, and M. Bhattacharya, “Quantum model of cooling and force sensing with an optically trapped nanoparticle,” *Optica* **3**, 318 (2016).
- [20] C. Sames, C. Hamsen, H. Chibani, P. A. Altin, T. Wilk, and G. Rempe, “Continuous parametric feedback cooling of a single atom in an optical cavity,” *Phys. Rev. A* **97**, 053404 (2018).
- [21] A. Ghosh, P. Kumar, C. Sommer, F. G. Jimenez, V. Sudhir, and C. Genes, “Theory of phase-adaptive parametric cooling,” *Phys. Rev. A* **107**, 053521 (2023).
- [22] S. Chakraborty, G. K. L. Wong, F. Oda, V. Wachter, S. V. Kusminskiy, T. Yokosawa, S. Hübner, B. A. Zubiri, E. Spiecker, M. Distaso, P. S. J. Russell, and N. Y. Joly, “Optomagnetic forces on YIG/YFeO<sub>3</sub> microspheres levitated in chiral hollow-core photonic crystal fibre,” (2024), [arXiv:2404.16182 \[physics.optics\]](https://arxiv.org/abs/2404.16182).
- [23] C. Gonzalez-Ballester, M. Aspelmeyer, L. Novotny, R. Quidant, and O. Romero-Isart, “Levitodynamics: Levitation and control of microscopic objects in vacuum,” *Science* **374**, eabg3027 (2021).
- [24] F. Benabid, J. C. Knight, and P. S. J. Russell, “Particle levitation and guidance in hollow-core photonic crystal fiber,” *Opt. Express* **10**, 1195–1203 (2002).
- [25] M. J. Renn, D. Montgomery, O. Vdovin, D. Z. Anderson, C. E. Wieman, and E. A. Cornell, “Laser-guided atoms in hollow-core optical fibers,” *Phys. Rev. Lett.* **75**, 3253–3256 (1995).
- [26] D. S. Bykov, O. A. Schmidt, T. G. Euser, and P. S. J. Russell, “Flying particle sensors in hollow-core photonic crystal fibre,” *Nature Photonics* **9**, 461–465 (2015).
- [27] D. S. Bykov, S. Xie, R. Zeltner, A. Machnev, G. K. L. Wong, T. G. Euser, and P. S. Russell, “Long-range optical trapping and binding of microparticles in hollow-core photonic crystal fibre,” *Light: Science & Applications* **7**, 22 (2018).
- [28] A. Sharma, S. Xie, and P. S. Russell, “Reconfigurable millimeter-range optical binding of dielectric microparticles in hollow-core photonic crystal fiber,” *Opt. Lett.* **46**, 3909–3912 (2021).
- [29] R. Zeltner, D. S. Bykov, S. Xie, T. G. Euser, and P. S. Russell, “Fluorescence-based remote irradiation sensor in liquid-filled hollow-core photonic crystal fiber,” *Applied Physics Letters* **108**, 231107 (2016).
- [30] X. Zhang, C.-L. Zou, L. Jiang, and H. X. Tang, “Cavity magnomechanics,” *Science Advances* **2**, e1501286 (2016).
- [31] V. Cherepanov, I. Kolokolov, and V. L’vov, “The saga of yig: Spectra, thermodynamics, interaction and relaxation of magnons in a complex magnet,” *Physics Reports* **229**, 81–144 (1993).
- [32] B. Zare Rameshti, S. Viola Kusminskiy, J. A. Haigh, K. Usami, D. Lachance-Quirion, Y. Nakamura, C.-M. Hu, H. X. Tang, G. E. Bauer, and Y. M. Blanter, “Cavity magnonics,” *Physics Reports* **979**, 1–61 (2022).
- [33] F. Ricci, *Levitodynamics toward force nano-sensors in vacuum* (Tesi doctoral, UPC, Institut de Ciències Fotòniques, 2019).
- [34] C. Genes, D. Vitali, P. Tombesi, S. Gigan, and M. Aspelmeyer, “Ground-state cooling of a micromechanical oscillator: Comparing cold damping and cavity-assisted cooling schemes,” *Phys. Rev. A* **77**, 033804 (2008).
- [35] K. Jacobs, *Quantum Measurement Theory and its Applications* (Cambridge University Press, Cambridge, 2014).
- [36] T. Corbitt, Y. Chen, E. Innerhofer, H. Müller-Ebhardt, D. Ottaway, H. Rehbein, D. Sigg, S. Whitcomb, C. Wipf, and N. Mavalvala, “An all-optical trap for a gram-scale mirror,” *Phys. Rev. Lett.* **98**, 150802 (2007).
- [37] T. Corbitt, C. Wipf, T. Bodiya, D. Ottaway, D. Sigg, N. Smith, S. Whitcomb, and N. Mavalvala, “Optical dilution and feedback cooling of a gram-scale oscillator to 6.9 mk,” *Phys. Rev. Lett.* **99**, 160801 (2007).
- [38] D. K. Hutchins, M. H. Harper, and R. L. Felder, “Slip correction measurements for solid spherical particles by modulated dynamic light scattering,” *Aerosol Science and Technology* **22**, 202–218 (1995).
- [39] S. Sharma, V. A. S. V. Bittencourt, A. D. Karenowska, and S. V. Kusminskiy, “Spin cat states in ferromagnetic insulators,” *Phys. Rev. B* **103**, L100403 (2021).
- [40] V. Wachter, V. A. S. V. Bittencourt, S. Xie, S. Sharma, N. Joly, P. S. Russell, F. Marquardt, and S. V. Kusminskiy, “Optical signatures of the coupled spin-mechanics of a levitated magnetic microparticle,” *J. Opt. Soc. Am. B* **38**, 3858–3871 (2021).
- [41] L. Magrini, V. A. Camarena-Chávez, C. Bach, A. Johnson, and M. Aspelmeyer, “Squeezed light from a levitated nanoparticle at room temperature,” *Phys. Rev. Lett.* **129**, 053601 (2022).



[42] S. Chigusa, T. Moroi, and K. Nakayama, “Detecting light boson dark matter through conversion into a magnon,” *Phys. Rev. D* **101**, 096013 (2020).

[43] M. Arndt and K. Hornberger, “Testing the limits of quantum mechanical superpositions,” *Nature Physics* **10**, 271–277 (2014).

[44] K. Jacobs, *Stochastic Processes for Physicists: Understanding Noisy Systems* (Cambridge University Press, 2010).

### Appendix A: Analytical solution for cooling rate

We start with the deterministic part of Eqs. (3) while neglecting the effect of noise

$$\frac{dq}{dt} = \Omega p \quad (\text{A1a})$$

$$\frac{dp}{dt} = -\gamma p - \Omega q - \beta\phi(t). \quad (\text{A1b})$$

Formally integrating the first equation gives

$$q(t) - q(t - \tau) = \Omega \int_{t-\tau}^t p(t') dt'. \quad (\text{A2})$$

Let us assume that the feedback is not affecting strongly over the time interval  $t - \tau$  to  $t$ . Then, to a first order, one can take into account that the natural evolution occurs at frequency  $\Omega$  and damping rate  $\gamma$ . This allows one to deterministically connect  $p(t')$  with  $p(t)$  and  $q(t)$

$$p(t') = \frac{\Omega}{\tilde{\Omega}} \left[ e^{(\gamma+\tilde{\Omega})(t-t')/2} - e^{(\gamma-\tilde{\Omega})(t-t')/2} \right] p(t) + \frac{1}{2\tilde{\Omega}} \left[ (\gamma + \tilde{\Omega}) e^{(\gamma+\tilde{\Omega})(t-t')/2} - (\gamma - \tilde{\Omega}) e^{(\gamma-\tilde{\Omega})(t-t')/2} \right] q(t), \quad (\text{A3})$$

where  $\tilde{\Omega} = \sqrt{\gamma^2 - 4\Omega^2}$ . After performing the integration of decaying, oscillating terms, one sees a renormalization of the decay rate from  $\gamma$  to  $\gamma + \bar{\Gamma}$  (by identifying the terms proportional to  $p(t)$ ) where

$$\bar{\Gamma} = \beta\mathcal{C} \left[ e^{\gamma\tau/2} \frac{\sinh \tilde{\Omega}\tau/2}{\tilde{\Omega}\tau/2} \right]. \quad (\text{A4})$$

In addition, the natural frequency is also modified from  $\Omega$  to  $\bar{\Omega}$  and can be identified from the extra factors in front of  $q(t)$  leading to

$$\bar{\Omega} = \Omega - \beta\mathcal{C} \left[ \frac{e^{\gamma\tau/2} \cosh(\tilde{\Omega}\tau/2) - 1}{\Omega\tau} \right] + \frac{\gamma\bar{\Gamma}}{2\Omega}. \quad (\text{A5})$$

In the limit of  $\tau \rightarrow 0$  i.e. when the derivative of the momentum is used to modify the motion, we have expected cold-damping type of result  $\bar{\Gamma} = \Gamma = \beta\mathcal{C}$  and the corresponding frequency of oscillation  $\bar{\Omega} = \Omega$ .

For an under-damped oscillator  $\gamma \ll \Omega$ , the expressions for the modified optical damping and frequency govern the following form

$$\bar{\Gamma} = \beta\mathcal{C} \left[ e^{\gamma\tau/2} \frac{\sin \Omega\tau}{\Omega\tau} \right], \quad (\text{A6})$$

$$\bar{\Omega} = \Omega - \beta\mathcal{C} \left[ \frac{e^{\gamma\tau/2} \cos(\Omega\tau) - 1}{\Omega\tau} \right]. \quad (\text{A7})$$

With the modified optical damping and frequency, the solution to Eqs. (A1) is governed by

$$q(t) = \frac{e^{-\bar{\gamma}t/2}}{\tilde{\bar{\Omega}}} \left[ \left( \bar{\gamma} \sinh(\tilde{\bar{\Omega}}t/2) + \tilde{\bar{\Omega}} \cosh(\tilde{\bar{\Omega}}t/2) \right) q_0 + \left( 2\tilde{\bar{\Omega}} \sinh(\tilde{\bar{\Omega}}t/2) \right) p_0 \right], \quad (\text{A8})$$

$$p(t) = \frac{e^{-\bar{\gamma}t/2}}{\tilde{\bar{\Omega}}} \left[ \left( -\bar{\gamma} \sinh(\tilde{\bar{\Omega}}t/2) + \tilde{\bar{\Omega}} \cosh(\tilde{\bar{\Omega}}t/2) \right) p_0 - \left( 2\tilde{\bar{\Omega}} \sinh(\tilde{\bar{\Omega}}t/2) \right) q_0 \right], \quad (\text{A9})$$

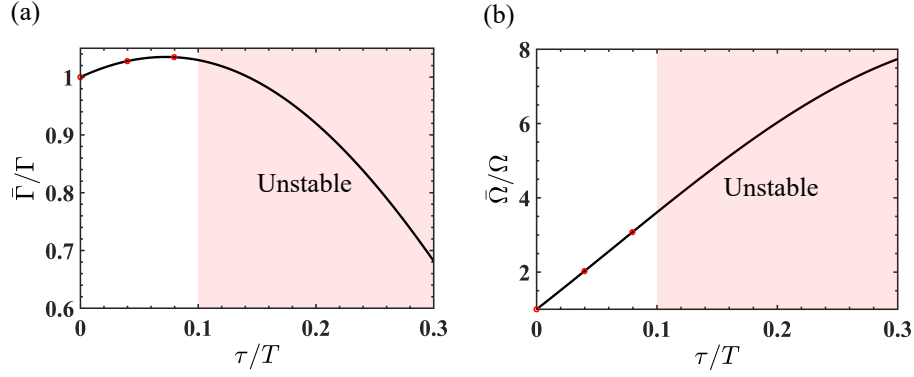


FIG. 8. Variation of the modified (a) optical damping rate and (b) frequency as a function of  $\tau/T$  where  $T = 2\pi/\Omega$  and  $\Omega = 2\pi \times 1$  kHz. The parameters used are  $\gamma = 0.3\Omega$ ,  $\beta/2\pi = 102$  MHz,  $\mathcal{C} = \mathcal{C}_{max} = 7.9 \times 10^{-5}$ . The analytical result and a few numerical checks shown as red dots confirm the predicted behavior. The shaded part represents the region where system becomes unstable.

where  $\tilde{\Omega} = \sqrt{\tilde{\gamma}^2 - 4\tilde{\Omega}^2}$ . From Eqs. (A8-A9), the phonon occupation can be written as

$$\bar{n}(t) = \frac{e^{-\tilde{\gamma}t}}{2\tilde{\Omega}^2} \left[ (q_0^2 + p_0^2) (\tilde{\gamma}^2 \cosh(\tilde{\Omega}t) - 4\tilde{\Omega}^2) + \tilde{\gamma}\tilde{\Omega}(q_0^2 - p_0^2) \sinh(\tilde{\Omega}t) + 8q_0p_0\tilde{\Omega}\tilde{\gamma} \sinh^2(\tilde{\Omega}t/2) \right]. \quad (\text{A10})$$

In Fig. 8, we depict the modified optical damping and frequency as a function of  $\tau/T$ . The predicted behavior of the modified damping rate and frequency can be checked by deducing its values for different  $\tau$  from fitting the occupancy given in Eq. (A10) with the numerical solution of Eqs. (A1). This is confirmed by the red circles shown in Fig. 8. Further, the shaded part in Fig. 8 governs the regime where the system becomes unstable.

## Appendix B: Classical stochastic evolution: thermal and measurement noise

We first analyze the thermal noise in order to get the hang of it. Afterwards, we will show how to compute the final occupancy by correlations of the measurement noise.

### 1. Thermal noise

The coupled difference equations for a harmonic oscillator undergoing damping

$$dq = \Omega p dt, \quad (\text{B1a})$$

$$dp = -\gamma p dt - \Omega q dt + \sqrt{2\gamma n_{\text{th}}} dW(t), \quad (\text{B1b})$$

can be turned into a set of recurrence equations. We discretize the time interval  $[0, t]$  into  $n$  steps of duration  $dt = t/n$  and can then rewrite the equations above as

$$\mathbf{v}_n - \mathcal{M}\mathbf{v}_{n-1} = \sqrt{2\gamma n_{\text{th}}}\mathbf{u}dW_{n-1}, \quad (\text{B2})$$

where  $\mathbf{v} = (q, p)^\top$  and  $\mathbf{u} = (0, 1)^\top$  and the evolution matrix is defined as

$$\mathcal{M} = \begin{bmatrix} 1 & \Omega dt \\ -\Omega dt & 1 - \gamma dt \end{bmatrix}. \quad (\text{B3})$$

The eigenvalues and eigenvectors of  $\mathcal{M}$  are

$$\lambda_{\pm} = 1 - \frac{\gamma_{\pm} dt}{2}; \quad \alpha_{\pm} = \begin{bmatrix} -\frac{\gamma_{\pm}}{2\tilde{\Omega}} \\ 1 \end{bmatrix}, \quad (\text{B4})$$

where  $\gamma_{\pm} = \gamma \left[ 1 \pm \sqrt{1 - \frac{4\Omega^2}{\gamma^2}} \right]$ . Now the diagonalization of the matrix  $\mathcal{M} = S\Lambda S^{-1}$  is straightforward in terms of its eigenvalues. The resulting quadratures after  $n$  steps are written as

$$q_n = \left( \frac{\gamma_+ \lambda_-^n - \gamma_- \lambda_+^n}{\gamma_+ - \gamma_-} \right) q_0 + \left( \frac{\gamma_- \gamma_+ (\lambda_-^n - \lambda_+^n)}{2\Omega(\gamma_+ - \gamma_-)} \right) p_0 + \left( \frac{\gamma_- \gamma_+}{2\Omega(\gamma_+ - \gamma_-)} \right) \sqrt{2\gamma n_{\text{th}}} \sum_{j=0}^{n-1} (\lambda_-^j - \lambda_+^j) dW_j \quad (\text{B5a})$$

$$p_n = \left( \frac{2\Omega(\lambda_+^n - \lambda_-^n)}{\gamma_+ - \gamma_-} \right) q_0 + \left( \frac{\gamma_+ \lambda_+^n - \gamma_- \lambda_-^n}{\gamma_+ - \gamma_-} \right) p_0 + \left( \frac{1}{\gamma_+ - \gamma_-} \right) \sqrt{2\gamma n_{\text{th}}} \sum_{j=0}^{n-1} (\gamma_+ \lambda_+^j - \gamma_- \lambda_-^j) dW_j, \quad (\text{B5b})$$

where the deterministic parts describe simply the oscillatory weakly damped transient evolution and the last terms are the effect of the thermal environment. In the large  $n$  limit we find a closed expression

$$q(t) = \left( \frac{\gamma_+ e^{-\gamma_- t/2} - \gamma_- e^{-\gamma_+ t/2}}{\gamma_+ - \gamma_-} \right) q_0 + \left( \frac{\gamma_- \gamma_+ (e^{-\gamma_- t/2} - e^{-\gamma_+ t/2})}{2\Omega(\gamma_+ - \gamma_-)} \right) p_0 + \left( \frac{\gamma_- \gamma_+}{2\Omega(\gamma_+ - \gamma_-)} \right) \sqrt{2\gamma n_{\text{th}}} \sum_{j=0}^{n-1} (\lambda_-^j - \lambda_+^j) dW_j, \quad (\text{B6a})$$

$$p(t) = \left( \frac{2\Omega(e^{-\gamma_+ t/2} - e^{-\gamma_- t/2})}{\gamma_+ - \gamma_-} \right) q_0 + \left( \frac{\gamma_+ e^{-\gamma_+ t/2} - \gamma_- e^{-\gamma_- t/2}}{\gamma_+ - \gamma_-} \right) p_0 + \left( \frac{1}{\gamma_+ - \gamma_-} \right) \sqrt{2\gamma n_{\text{th}}} \sum_{j=0}^{n-1} (\gamma_+ \lambda_+^j - \gamma_- \lambda_-^j) dW_j, \quad (\text{B6b})$$

where we have used that  $\lim_{n \rightarrow \infty} (1 - \gamma_{\pm} t/2n)^n = e^{-\gamma_{\pm} t/2}$ . From these expressions, one can estimate that in steady state  $\langle q^2 \rangle_{\text{ss}} = \langle p^2 \rangle_{\text{ss}} = n_{\text{th}}$  by using  $\langle dW_j dW_{j'} \rangle = \delta_{jj'} dt/n$  and evaluating the limit

$$\lim_{n \rightarrow \infty} \sum_{j=0}^{n-1} \lambda_{\pm}^{2j} = \frac{1}{\gamma_{\pm} dt}, \quad (\text{B7a})$$

$$\lim_{n \rightarrow \infty} \sum_{j=0}^{n-1} \lambda_+^j \lambda_-^j = \frac{2}{(\gamma_+ + \gamma_-) dt}. \quad (\text{B7b})$$

## 2. Measurement noise

To this end we start with the noise propagating via  $-\beta\phi(t)dt$  in Eqs. (3). This measurement backaction can be written as a Wiener process in the difference equations form as

$$\mathcal{N}^{\text{det}}(t) = -\frac{\eta\beta\mathcal{C}}{\Omega} \left[ \frac{W^{\text{det}}(t) - W^{\text{det}}(t - \tau)}{\tau} \right] dt. \quad (\text{B8})$$

and to be added to the standard thermal noise  $\sqrt{2\gamma n_{\text{th}}} dW^{\text{th}}(t)$ . The above Wiener process can further be expressed as a discrete sum over Wiener increments with infinitesimal increment of time step  $dt$  such that  $t = ndt$  and  $\tau = n_{\tau} dt$ , we can express the measurement noise as

$$\mathcal{N}^{\text{det}}(t) = -\mathcal{A} \sum_{m=1}^{n_{\tau}} dW_{n-n_{\tau}+m}^{\text{det}}, \quad (\text{B9})$$

where we make the notation  $\mathcal{A} = \eta\beta\mathcal{C}dt/(\Omega\tau)$ . From here, we follow the derivation given in Ref. [21] to determine the contribution of thermal and detection noises to the steady solution that can be obtained, for  $p_{ss}(t)$ , as a limit of  $p_n$  for large  $n$

$$p_n = \frac{1}{\bar{\gamma}_+ - \bar{\gamma}_-} \sum_{j=0}^{n-1} \left( \mathcal{N}_j^{\text{det}} + \sqrt{2\gamma n_{\text{th}}} dW_j^{\text{th}} \right) \left( \bar{\gamma}_+ \bar{\lambda}_+^j - \bar{\gamma}_- \bar{\lambda}_+^j \right), \quad (\text{B10})$$

where  $\bar{\lambda}_{\pm} = 1 - \bar{\gamma}_{\pm} dt/2$  and  $\bar{\gamma}_{\pm} = \bar{\gamma} \left[ 1 \pm \sqrt{1 - \frac{4\Omega^2}{\bar{\gamma}^2}} \right]$  contain a modified damping  $\bar{\gamma} = \gamma + \bar{\Gamma}$ , and frequency  $\bar{\Omega}$ . Now our task is to compute the variance  $\langle p_n^2 \rangle$  in steady state. For two uncorrelated noises one can split this into

$\langle p_n^2 \rangle = \langle p_n^2 \rangle^{\text{th}} + \langle p_n^2 \rangle^{\text{det}}$ . Let's first estimate the contribution from thermal noise,  $\langle p_n^2 \rangle^{\text{th}}$ , as an exercise. We use  $\langle dW_j^{\text{th}} dW_{j'}^{\text{th}} \rangle = dt \delta_{jj'}$  and evaluate sum  $\lim_{n \rightarrow \infty} \sum_{j=0}^{n-1} \bar{\lambda}_{\pm}^{2j} = 1/(\bar{\gamma}_{\pm} dt)$ , and  $\lim_{n \rightarrow \infty} \sum_{j=0}^{n-1} \bar{\lambda}_+^j \bar{\lambda}_-^j = \frac{2}{(\bar{\gamma}_+ + \bar{\gamma}_-) dt}$  (for details see previous section). This gives the expected estimate of the thermal final occupancy

$$\langle p_n^2 \rangle^{\text{th}} = \frac{\gamma n_{\text{th}}}{\gamma + \bar{\Gamma}} \left( \frac{\Omega}{\bar{\Omega}} \right). \quad (\text{B11})$$

Now to evaluate the contribution of measurement backaction, we write the steady state correlations stemming from the detection noise as

$$\langle p_n^2 \rangle^{\text{det}} = \frac{1}{(\bar{\gamma}_+ - \bar{\gamma}_-)^2} \sum_{j=0}^{n-1} \sum_{j'=0}^{n-1} \langle \mathcal{N}_j^{\text{det}} \mathcal{N}_{j'}^{\text{det}} \rangle (\bar{\gamma}_+ \bar{\lambda}_+^j - \bar{\gamma}_- \bar{\lambda}_+^j) (\bar{\gamma}_+ \bar{\lambda}_+^{j'} - \bar{\gamma}_- \bar{\lambda}_+^{j'}). \quad (\text{B12})$$

Using Eq. (B9), this leads to

$$\langle p_n^2 \rangle^{\text{det}} = \frac{\mathcal{A}^2}{(\bar{\gamma}_+ - \bar{\gamma}_-)^2} \sum_{j,j'=0}^{n-1} \sum_{m,m'=0}^{n_{\tau}} (\bar{\gamma}_+ \bar{\lambda}_+^j - \bar{\gamma}_- \bar{\lambda}_+^j) (\bar{\gamma}_+ \bar{\lambda}_+^{j'} - \bar{\gamma}_- \bar{\lambda}_+^{j'}) \langle dW_{j-n_{\tau}+m}^{\text{det}} dW_{j'-n_{\tau}+m'}^{\text{det}} \rangle. \quad (\text{B13})$$

The correlations of the detection noise will impose the constraint  $j + m = j' + m'$  and the expression above reduces to

$$\langle p_n^2 \rangle^{\text{det}} = \frac{\mathcal{A}^2 dt}{(\bar{\gamma}_+ - \bar{\gamma}_-)^2} \sum_{j=0}^{n-1} \sum_{m,m'=0}^{n_{\tau}} \left[ \bar{\gamma}_+^2 \bar{\lambda}_+^{2j} + \bar{\gamma}_-^2 \bar{\lambda}_-^{2j} - \bar{\gamma}_- \bar{\gamma}_+ \bar{\lambda}_+^j \bar{\lambda}_-^j (\bar{\lambda}_-^{m-m'} + \bar{\lambda}_+^{m-m'}) \right]. \quad (\text{B14})$$

Evaluating the summation over  $j$  leads to

$$\langle p_n^2 \rangle^{\text{det}} = \frac{\mathcal{A}^2}{(\bar{\gamma}_+ - \bar{\gamma}_-)(\bar{\gamma}_+ + \bar{\gamma}_-)} \sum_{m,m'=0}^{n_{\tau}} \left[ \bar{\gamma}_+ \bar{\lambda}_+^{m-m'} - \bar{\gamma}_- \bar{\lambda}_-^{m-m'} \right]. \quad (\text{B15})$$

The summation over  $m$  and  $m'$  gives  $\sum_{m,m'=1}^{n_{\tau}} \bar{\lambda}_{\pm}^{m-m'} = \frac{4\bar{\lambda}_{\pm}}{(\bar{\lambda}_{\pm}-1)^2} \sinh^2(\bar{\gamma}_{\pm}\tau/4)$ . Using this and inserting the expressions of  $\bar{\lambda}_{\pm}$ ,  $\bar{\gamma}_{\pm}$  and  $\mathcal{A}$  and after some algebraic simplifications, we obtain following expression for the variance due to the detection noise

$$\langle p_n^2 \rangle^{\text{det}} = \left[ \frac{\eta\beta\mathcal{C}}{2\Omega} \right]^2 \frac{1}{\bar{\gamma}_+ \sqrt{\bar{\gamma}_+^2 - 4\bar{\Omega}^2}} \left[ \bar{\gamma}_+ \left( \frac{\sinh\left(\frac{\bar{\gamma}_+\tau}{4}\right)}{\bar{\gamma}_+\tau/4} \right)^2 - \bar{\gamma}_- \left( \frac{\sinh\left(\frac{\bar{\gamma}_-\tau}{4}\right)}{\bar{\gamma}_-\tau/4} \right)^2 \right]. \quad (\text{B16})$$

Eventually, the total variance can be written

$$\langle p_n^2 \rangle = \frac{\gamma n_{\text{th}}}{\gamma + \bar{\Gamma}} \left( \frac{\Omega}{\bar{\Omega}} \right) + \left[ \frac{\eta\beta\mathcal{C}}{2\Omega} \right]^2 \frac{1}{\bar{\gamma}_+ \sqrt{\bar{\gamma}_+^2 - 4\bar{\Omega}^2}} \left[ \bar{\gamma}_+ \left( \frac{\sinh\left(\frac{\bar{\gamma}_+\tau}{4}\right)}{\bar{\gamma}_+\tau/4} \right)^2 - \bar{\gamma}_- \left( \frac{\sinh\left(\frac{\bar{\gamma}_-\tau}{4}\right)}{\bar{\gamma}_-\tau/4} \right)^2 \right]. \quad (\text{B17})$$

The second term basically tells us how much the effective temperature is modified via measurement backaction.

#### a. Under-damped oscillator

Let us obtain a simplified expression of the variance of the measurement back action for the case of under-damped oscillator i.e.  $\bar{\gamma} \ll \bar{\Omega}$ . In this case,  $\bar{\gamma}_+ = 2i\bar{\Omega}$ , and  $\bar{\gamma}_- = -2i\bar{\Omega}$ . Using this in Eq. (B16) gives

$$\langle p_n^2 \rangle^{\text{det}} = \frac{1}{\gamma + \bar{\Gamma}} \times \left[ \frac{\eta\beta\mathcal{C}}{\sqrt{2}\Omega} \times \frac{\sin\left(\frac{\bar{\Omega}\tau}{2}\right)}{\bar{\Omega}\tau/2} \right]^2. \quad (\text{B18})$$

#### b. Over-damped oscillator

For an over-damped situation,  $\bar{\gamma} \gg \bar{\Omega}$ . In this case,  $\bar{\gamma}_+ = 2\bar{\gamma}$ , and  $\bar{\gamma}_- \approx 0$ . The expression for the variance of the detection noise is then governed by

$$\langle p_n^2 \rangle^{\text{det}} = \frac{1}{\gamma + \bar{\Gamma}} \times \left[ \frac{\eta\beta\mathcal{C}}{\sqrt{2}\Omega} \times \frac{\sinh\left(\bar{\gamma}\tau/2\right)}{\bar{\gamma}\tau/2} \right]^2. \quad (\text{B19})$$



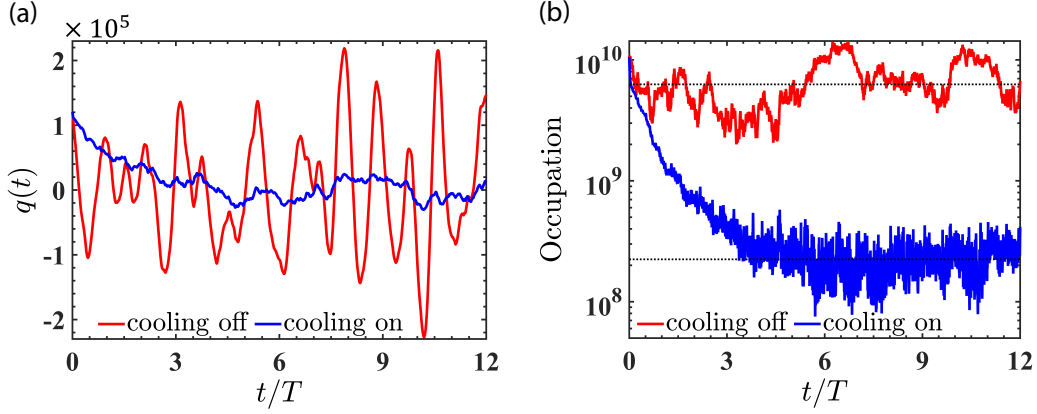


FIG. 9. Temporal evolution of the phonon occupancy in the absence (solid red line) and presence (solid blue line) of cooling scheme. The Occupancy is obtained from the numerical simulation of Eqs. (C1a-C1b). The dotted lines show the validity of the analytically predicted final occupancy given by Eq. (17). Here  $\gamma/2\pi = 300$  Hz and rest of the parameters are same as in Fig. 6.

### Appendix C: Numerical procedure

Now we describe the numerical procedure to obtain the mechanical oscillator dynamics in the presence of thermal and measurement noise. For this, we write the following coupled difference equations

$$dq = \Omega p dt, \quad (\text{C1a})$$

$$dp = -\gamma p dt - \Omega q dt - \frac{\beta C}{\Omega} \left( \frac{q(t) - q(t - \tau)}{\tau} \right) dt + \sqrt{2\gamma n_{\text{th}}} dW^{\text{th}}(t) - \mathcal{A} \sum_{m=1}^{n_\tau} dW_{n-n_\tau+m}^{\text{det}}, \quad (\text{C1b})$$

where the action of the thermal bath is included as a Wiener process  $dW^{\text{th}}(t)$  of zero average and variance equal to numerical time  $dt$ . Numerically, we can express the Wiener increments in terms of a Gaussian distribution [44] as  $dW^{\text{th}}(t) = \sqrt{dt}\mathcal{N}(0, 1)$ , where  $\mathcal{N}(0, 1)$  represents a normal distribution of unit variance from which a random variable is to be drawn. On the other hand, the last term in Eq. (C1b) represents Wiener process entering during the measurement process and is written as a discrete sum over the Wiener increments with increment of time  $dt$ . Numerically, we model it as  $\sum_{m=1}^{n_\tau} dW_{n-n_\tau+m}^{\text{det}} = \sqrt{\tau} \sum_{m=1}^{n_\tau} \mathcal{N}_m$ , where  $\mathcal{N}_m$  is a random number drawn from a normal distribution at each time evolution step. To numerically solve Eqs. (C1a-C1b), we use the Runge-Kutta fourth-order (RK4) method with a time step  $dt = 10^{-4}/\Omega$  that ensure the numerical stability.

Using above numerical procedure, we simulate the difference equations for an oscillator undergoing thermalization at a rate  $\gamma = 0.3\Omega$  with a thermal environment of effective occupancy  $n_{\text{th}} = 6.2 \times 10^9$  (C1a-C1b). Fig. 9(a) shows the resulting position dynamics while Fig. 9(b) gives the phonon occupancy. These results are plotted both in the absence and presence of cooling scheme. As shown in Fig. 9, in the absence of the proposed cooling scheme, the system quickly attains equilibrium with its thermal environment thereby attaining a high thermal phonon-occupancy governed by  $\bar{n} = n_{\text{th}}$ . However, when the phase-adaptive feedback cooling is switched on for  $\tau/T = 1.6 \times 10^{-5}$ , the initial high phonon occupancy decays and eventually it saturates at a final value  $\bar{n}$  governed by our analytical expression in Eq. (17).

### Appendix D: Estimation of imaging factor ( $\eta$ )

Our phase-adaptive mechanism is based on the detection of particle's position which can be deduced as  $y_{\text{det}}(t) = y(t) + y_{zpm}\eta W^{\text{det}}(t)$ . Here the estimated position is written as a sum of the true position  $y(t)$  and detection noise which is modelled in terms of Wiener process. To find out the detection noise amplitude  $\eta$ , we write the position power spectral density  $S_{\text{det}}(\omega) = S_y^{\text{th}}(\omega) + y_{zpm}^2 \eta^2 S_W(\omega)$ . Here, the first term is the thermal noise contribution written as:

$$S_y(\omega) = \frac{2k_B T_{\text{th}} \gamma / m}{(\omega^2 - \Omega^2)^2 + \gamma^2 \omega^2}, \quad (\text{D1})$$

whereas the second term in  $S_{\text{det}}$  represents a contribution from the detection noise that sets the noise floor in the measurement. Note that the various terms involved in Eq. (D1) are already defined in Sec. II. Now, to obtain contribution of detection noise, we write the finite Fourier transform of the Wiener process over a measurement time window  $T_w$  as follows

$$\tilde{W}^{\text{det}}(\omega, T_w) = \int_0^{T_w} W^{\text{det}}(t) e^{-i\omega t} dt. \quad (\text{D2})$$

The sampled spectral density of the Wiener process can then be estimated as

$$S_W(\omega) = \frac{1}{T_w} \langle (\tilde{W}^{\text{det}})^*(\omega, T_w) \tilde{W}^{\text{det}}(\omega, T_w) \rangle. \quad (\text{D3})$$

Using Eq. (D2) in Eq. (D3), we can write

$$S_W(\omega) = \frac{1}{T_w} \int_0^{T_w} \int_0^{T_w} \langle W^{\text{det}}(t') W^{\text{det}}(t'') \rangle e^{-i\omega(t''-t')} dt'' dt'. \quad (\text{D4})$$

Changing the region of integration in above equation, we get

$$S_W(\omega) = \frac{1}{T_w} \int_0^{T_w} \int_0^{t'} \langle W^{\text{det}}(t') W^{\text{det}}(t'') \rangle e^{-i\omega(t''-t')} dt'' dt' + \frac{1}{T_w} \int_0^{T_w} \int_{t'}^{T_w} \langle W^{\text{det}}(t') W^{\text{det}}(t'') \rangle e^{-i\omega(t''-t')} dt'' dt'. \quad (\text{D5})$$

For a Wiener process, two time correlation function is expressed as  $\langle W^{\text{det}}(t') W^{\text{det}}(t'') \rangle = \min(t', t'')$ . For  $0 \leq t'' \leq t'$ ,  $\langle W^{\text{det}}(t') W^{\text{det}}(t'') \rangle = t''$  and for  $t' \leq t'' \leq T_w$ ,  $\langle W^{\text{det}}(t') W^{\text{det}}(t'') \rangle = t'$ . Using this and performing the integration, the spectral contribution due to detection noise in the large  $T_w$  takes following form

$$S_W(\omega) \approx \frac{2}{\omega^2}. \quad (\text{D6})$$

The estimated noise floor for the detection scheme under consideration is  $7.5 \text{ pm}/\sqrt{\text{Hz}}$ . Around  $\omega \approx \Omega$  and using Eq. (D6), we find  $\eta = \frac{7.5\Omega}{y_{z\text{pm}}\sqrt{2}} \frac{\text{pm}}{\sqrt{\text{Hz}}}$ .

---